Nonadditive three-body potential and third to eighth virial coefficients of carbon dioxide

Robert Hellmann

Citation: J. Chem. Phys. **146**, 054302 (2017); doi: 10.1063/1.4974995
View online: http://dx.doi.org/10.1063/1.4974995
View Table of Contents: http://aip.scitation.org/toc/jcp/146/5
Published by the American Institute of Physics

Nonadditive three-body potential and third to eighth virial coefficients of carbon dioxide

Robert Hellmann[a)]
Institut für Chemie, Universität Rostock, 18059 Rostock, Germany

(Received 30 November 2016; accepted 16 January 2017; published online 2 February 2017)

A new nonadditive three-body interaction potential for carbon dioxide was determined from supermolecular *ab initio* calculations up to the coupled cluster with single, double, and perturbative triple excitations [CCSD(T)] level of theory for 9401 configurations. A physically motivated analytical function with terms for describing nonadditive dispersion, induction, and exchange contributions was fitted to the calculated nonadditive three-body interaction energies. For the 7996 configurations with a total interaction energy of less than 3000 K, the mean absolute error of the analytical function is 0.32 K. The new nonadditive three-body potential was applied together with a previously published pair potential [R. Hellmann, Chem. Phys. Lett. **613**, 133 (2014)] to calculate the third to seventh virial coefficients of CO_2 at subcritical and supercritical temperatures up to 2000 K. The eighth virial coefficient was also calculated, but using only the pair potential and only at temperatures from 600 K to 2000 K because of the enormous computational costs. A simple analytical function was fitted individually to the calculated values of each virial coefficient, including previously determined values of the second virial coefficient, to obtain an analytical virial equation of state (VEOS). For densities at which the VEOS is converged, the agreement in pressure with the reference EOS of Span and Wagner [J. Phys. Chem. Ref. Data **25**, 1509 (1996)] is mostly within ±0.5%. However, for temperatures above about 700 K, much larger deviations occur at higher densities, which we ascribe mainly to deficiencies of the reference EOS due to the lack of accurate data for these experimentally difficult conditions. *Published by AIP Publishing.* [http://dx.doi.org/10.1063/1.4974995]

I. INTRODUCTION

The calculation of the thermophysical properties of a fluid requires precise knowledge of the potential energy surface (PES) describing the interactions between individual molecules. For dilute gases, the thermophysical properties are governed solely by binary interactions and therefore by the pair potentials, which can be determined with high accuracy for atoms[1–3] or small molecules[4–10] using quantum-chemical *ab initio* methods. Provided that the pair potential functions are available, it is straightforward to calculate, for example, the second virial coefficient using statistical thermodynamics or the transport properties in the limit of zero density employing the kinetic theory of gases.[11–13]

At higher densities, many-body effects strongly influence the macroscopic properties of a fluid. The most common way to account for this is the implicit inclusion of many-body effects into the pair potentials. These so-called effective pair potentials are usually adjusted to structural properties of the molecules and experimental data for bulk properties. Effective pair potentials are computationally efficient, but they do not represent the underlying physics of the interactions correctly. Therefore, their predictive capability is limited. The physically correct approach is a many-body expansion of the total interaction potential V_N of an N-particle system,

$$V_N = \sum_{i<j} V_{ij} + \sum_{i<j<k} \Delta V_{ijk} + \ldots, \tag{1}$$

where V_{ij} is the pair potential between particles i and j, and ΔV_{ijk} is the nonadditive three-body potential between particles i, j, and k,

$$\Delta V_{ijk} = V_{ijk} - V_{ij} - V_{ik} - V_{jk}. \tag{2}$$

Here, V_{ijk} denotes the total interaction potential between the three particles. The nonadditive three-body potential can be determined using quantum-chemical *ab initio* methods in a similar way as the pair potential, though the increased dimensionality of the PES makes this more difficult. For CO_2, such investigations have been carried out by Oakley and Wheatley[14] and by Yu and Schmidt.[15] Other substances that have been extensively studied include helium,[16–18] argon,[19–22] and water.[23–26]

The equation of state (EOS) of a fluid can be determined from intermolecular PESs by means of molecular dynamics (MD) or Monte Carlo (MC) simulations of a large number of particles in a box with periodic boundary conditions. In the case of gases and supercritical fluids, an alternative route to the EOS is provided by the virial expansion,

$$\frac{p}{\rho_m RT} = 1 + B_2(T)\rho_m + B_3(T)\rho_m^2 + \ldots, \tag{3}$$

where p is the pressure, ρ_m is the molar density, R is the universal gas constant, T is the temperature, and B_n is the nth virial coefficient. For rigid particles, the classical nth virial coefficient can be written as a multidimensional integral over the positions and orientations of n particles, with the integrand depending on the temperature and the two-body to n-body potentials, see Ref. 27 and references therein. Hereafter, a virial

a)Electronic mail: robert.hellmann@uni-rostock.de

EOS (VEOS) truncated after the nth virial coefficient will be referred to as an nth-order VEOS or, following Ref. 28, as VEOSn. For argon, Jäger *et al.*[21] have shown that a seventh-order VEOS based on *ab initio* two-body and nonadditive three-body potentials can be almost as accurate as the best experimental data at densities at which the virial expansion is converged. Shaul *et al.*[29] have argued that virial coefficients of helium calculated from the best available *ab initio* two-body and nonadditive three-body potentials are even accurate enough to be used in gas metrology.

In this work, we present a new nonadditive three-body potential for CO_2. It is based on quantum-chemical *ab initio* calculations up to the coupled cluster with single, double, and perturbative triple excitations [CCSD(T)][30] level of theory for 9401 points on the PES. This represents a significant improvement compared with the nonadditive three-body potentials of Oakley and Wheatley[14] and of Yu and Schmidt,[15] which are based on only 250 and 200 points, respectively, calculated at lower levels of theory. The new nonadditive three-body potential has been used together with our recent CO_2–CO_2 potential[9] (which yielded excellent agreement with the best experimental data for the second virial coefficient and the dilute gas transport properties[9]) to calculate the third to seventh virial coefficients of carbon dioxide at subcritical and supercritical temperatures up to 2000 K. The eighth virial coefficient has been calculated using only the pair potential and only at temperatures from 600 K to 2000 K because of the enormous computational costs. For all virial coefficients, the integrations over the positions and orientations of the molecules have been carried out by means of the Mayer-sampling Monte Carlo (MSMC) method of Singh and Kofke.[31] Finally, an analytical VEOS8 has been constructed by fitting a simple analytical function individually to the calculated values of each virial coefficient, including the previously determined values of the second virial coefficient.[9]

The paper is organized as follows. In Sec. II, the new nonadditive three-body potential is presented. In Sec. III, the computational method for the determination of the virial coefficients is summarized, and the results for the third virial coefficient and the VEOS up to eighth order are compared with selected experimental data and experimentally based EOSs. A summary and conclusions are given in Sec. IV.

II. NONADDITIVE THREE-BODY POTENTIAL

A. Internal coordinates and grid points

The internal coordinates used to describe all possible relative configurations of three rigid CO_2 molecules are defined as follows. The C atom of molecule 1 is located at the origin of a Cartesian coordinate system. The C atom of molecule 2 is located on the x axis at $x = R_{12}$. The C atom of molecule 3 is initially located on the x axis at $x = R_{13}$ and then rotated counterclockwise in the xy plane about the origin by the angle $\bar{\theta}_1$. The spatial orientation of the ith molecule is described by the polar angles θ_i and ϕ_i. As in our previous work on the CO_2–CO_2 PES,[9] the CO_2 molecules are approximated as rigid rotors using the zero-point vibrationally averaged geometry, which is characterized by a CO bond length of 1.1625 Å[9] and a bond angle of 180°. Thus, the nonadditive three-body potential is a nine-dimensional PES,

$$\Delta V_{123} = \Delta V_{123}(R_{12}, R_{13}, \bar{\theta}_1, \theta_1, \theta_2, \theta_3, \phi_1, \phi_2, \phi_3). \quad (4)$$

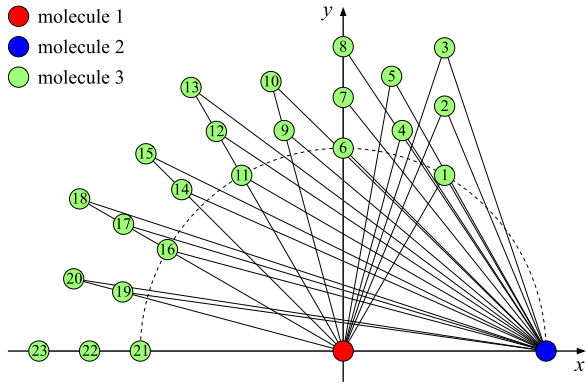

FIG. 1. Position of the C atom of molecule 3 relative to the positions of the C atoms of molecules 1 and 2 for the 23 selected triangular shapes defined by the ratio R_{13}/R_{12} and the interior angle $\bar{\theta}_1$.

The grid points were distributed in the following manner. First, 23 triangular shapes defined by the ratio R_{13}/R_{12} and the angle $\bar{\theta}_1$ were selected. Since all three molecules are identical, the shapes can be restricted such that $\bar{\theta}_1$ is the largest of the three interior angles and $R_{13}/R_{12} \geqslant 1$. The 23 chosen triangular shapes are visualized and labeled in Fig. 1. For all shapes, angular sets $\omega_{123} = (\theta_1, \theta_2, \theta_3, \phi_1, \phi_2, \phi_3)$ were then generated by varying the six angles in steps of 90°, starting at 0° for the three θ angles and at individually specified values for the three ϕ angles (e.g., $\phi_1 = 60°$, $\phi_2 = 30°$, and $\phi_3 = 0°$ for triangular shape 1, which is the equilateral triangle). The number of distinct angular sets ω_{123} resulting from this procedure varied between 10 for shapes 1 and 21 and 27 for shapes 4, 5, 7–10, 12–15, and 17–20. Between 20 and 50 further angular sets were generated randomly (with a uniform distribution in the three ϕ angles and in the cosines of the three θ angles) for each shape, except for shapes 3, 8, 13, 18, and 23. The latter five shapes should be the least important ones as they have the highest R_{13}/R_{12} ratios, which usually results in the two-body potential V_{12} dominating the interactions between the three molecules and hence the nonadditive contribution ΔV_{123} becoming unimportant. A total of 1196 combinations of a shape and an angular set ω_{123} were obtained in this way. Finally, four to twelve R_{12} values were selected for each of these combinations, resulting in 9401 unique configurations of three CO_2 molecules.

B. *Ab initio* calculations

The nonadditive three-body interaction energies ΔV_{123} were obtained using the supermolecular approach,

$$\begin{aligned}\Delta V_{123} &= V_{123} - V_{12} - V_{13} - V_{23} \\ &= E_{123} - E_1 - E_2 - E_3 - (E_{12} - E_1 - E_2) \\ &\quad - (E_{13} - E_1 - E_3) - (E_{23} - E_2 - E_3) \\ &= E_{123} - E_{12} - E_{13} - E_{23} + E_1 + E_2 + E_3, \end{aligned} \quad (5)$$

where E_{123} is the total electronic energy of the three interacting molecules, E_{ij} is the corresponding quantity for an isolated pair of molecules i and j in the same geometry as

in the three-molecule system, and E_i is the total electronic energy of an isolated molecule. To avoid the basis set superposition error, the counterpoise procedure[32] was applied, i.e., all electronic energies were calculated in the full basis set of the three-molecule system.

For all 9401 grid points, ΔV_{123} values were computed using resolution of identity second-order Møller–Plesset perturbation theory (RI-MP2)[33,34] with the RI-JK approximation[35,36] for the Hartree–Fock part. The aug-cc-pVQZ[37] basis set (abbreviated as aVQZ) and the VQZ-JKFIT[38] and aVQZ-MP2FIT[39] auxiliary basis sets were used for these calculations. We checked that the differences between ΔV_{123} values obtained using this approach and ΔV_{123} values obtained using the standard MP2 method are negligibly small. Since the MP2 and RI-MP2 approaches do not account for nonadditive dispersion, ΔV_{123} values were also calculated at the CCSD(T)[30]/aVTZ[37] level for all grid points and combined with the RI-MP2/aVQZ values such that an approximation to the CCSD(T)/aVQZ level was obtained,

$$\Delta V_{123} = \Delta V_{123}^{\text{RI-MP2/aVQZ}} + \Delta V_{123}^{\text{CCSD(T)/aVTZ}} - \Delta V_{123}^{\text{MP2/aVTZ}}. \tag{6}$$

The $\Delta V_{123}^{\text{MP2/aVTZ}}$ values were obtained as a byproduct of the CCSD(T)/aVTZ calculations. Both the RI-MP2 and the CCSD(T) calculations were performed within the frozen-core approximation.

The results of the *ab initio* calculations for the 9401 selected configurations of three CO_2 molecules can be found in the supplementary material. The ORCA[40] and CFOUR[41] programs were used for all RI-MP2 and CCSD(T) calculations, respectively, reported in this work.

C. Analytical potential function

A physically motivated analytical function, consisting of terms for describing nonadditive dispersion, induction, and exchange contributions, was fitted to the 9401 calculated nonadditive three-body interaction energies,

$$\Delta V_{123}^{\text{fit}} = \Delta V_{123}^{\text{disp}} + \Delta V_{123}^{\text{ind}} + \Delta V_{123}^{\text{exch}}. \tag{7}$$

The dispersion contribution $\Delta V_{123}^{\text{disp}}$ is given as a sum of Axilrod–Teller–Muto[42,43] (ATM) terms,

$$\Delta V_{123}^{\text{disp}} = \sum_{i=1}^{3}\sum_{j=1}^{3}\sum_{k=1}^{3} \frac{C_{9\,ijk}}{R_{12|ij}^3 R_{13|ik}^3 R_{23|jk}^3} \times \left(1 + 3\cos\bar{\theta}_{1|i}\cos\bar{\theta}_{2|j}\cos\bar{\theta}_{3|k}\right), \tag{8}$$

where i, j, and k are the indices of sites located in molecules 1, 2, and 3, respectively, $R_{12|ij}$ is the distance between site i of molecule 1 and site j of molecule 2, and $\cos\bar{\theta}_{1|i}$ is the interior angle at site i of molecule 1 of the triangle formed by sites i, j, and k of molecules 1, 2, and 3, respectively. The sites are located on the C atoms and on the CO bonds at a distance of 0.8 Å from the C atoms (which was found by trial and error to be the optimal value for the fit of ΔV_{123}). It is easily seen that this approach yields dispersion interactions that are isotropic with respect to the spatial orientations of the three molecules in the limit of very large separations between them. To minimize the negative impact of this unrealistic behavior, the four distinct $C_{9\,ijk}$ fit coefficients were constrained such that the isotropic C_9 dispersion coefficient of CO_2 resulting from this approach in the limit of very large separations, $C_{9\,\text{iso}} = \sum_{i=1}^{3}\sum_{j=1}^{3}\sum_{k=1}^{3} C_{9\,ijk}$, is equal to the isotropic average of the actual C_9 dispersion coefficient of CO_2 (1970 a.u.) obtained from dipole oscillator strength distributions.[44] Thus, there are only three independent $C_{9\,ijk}$ fit coefficients.

The induction contribution $\Delta V_{123}^{\text{ind}}$ is given as a sum of three terms,

$$\Delta V_{123}^{\text{ind}} = \Delta V_{1}^{\text{ind}} + \Delta V_{2}^{\text{ind}} + \Delta V_{3}^{\text{ind}}, \tag{9}$$

where $\Delta V_{1}^{\text{ind}}$ is the contribution due to dipole moments induced on the polarizable sites of molecule 1 by the electric field generated by molecules 2 and 3, with analogous definitions for the other two terms. We use three polarizable sites per molecule, which are the same as the ones used for $\Delta V_{123}^{\text{disp}}$. Assuming that one can neglect the contributions of the induced dipole moments of one molecule to the electric field at the polarizable sites of the other molecules and contributions to the induction energy due to hyperpolarizabilities, quadrupole polarizabilities, etc., $\Delta V_{1}^{\text{ind}}$ can be written as

$$\Delta V_{1}^{\text{ind}} = -\sum_{i=1}^{3} \mathbf{E}_{12|i}^{\mathrm{T}} \boldsymbol{\alpha}_{1|i} \mathbf{E}_{13|i}. \tag{10}$$

Here, $\boldsymbol{\alpha}_{1|i}$ is the polarizability tensor of site i of molecule 1 in the Cartesian coordinate system of the three-molecule system,

$$\boldsymbol{\alpha}_{1|i} = (\alpha_{i\parallel} - \alpha_{i\perp})\,\hat{\mathbf{n}}_1\hat{\mathbf{n}}_1^{\mathrm{T}} + \alpha_{i\perp}\mathbf{I}, \tag{11}$$

where $\alpha_{i\parallel}$ and $\alpha_{i\perp}$ are the polarizabilities of site i parallel and perpendicular to the molecular axis, respectively, $\mathbf{I}$ is the identity matrix, and $\hat{\mathbf{n}}_1$ is a unit vector along the molecular axis of molecule 1. The quantity $\mathbf{E}_{12|i}$ denotes the electric field at site i of molecule 1 generated by the permanent charge distribution of molecule 2. For simplicity, we approximate the charge distribution by point charges q at the three polarizable sites. Thus,

$$\mathbf{E}_{12|i} = -\sum_{j=1}^{3} q_j \frac{\mathbf{R}_{12|ij}}{R_{12|ij}^3}. \tag{12}$$

For consistency with the calculations presented in Sec. II B, the charges were chosen to reproduce the CO_2 quadrupole moment resulting from an *ab initio* calculation at the frozen-core CCSD(T)/aVQZ level (−3.164 24 a.u.), and the polarizabilities of CO_2 parallel and perpendicular to the molecular axis, $\alpha_\parallel = \sum_{i=1}^{3}\alpha_{i\parallel}$ and $\alpha_\perp = \sum_{i=1}^{3}\alpha_{i\perp}$, had to be equal to *ab initio* values calculated at the same level of theory ($\alpha_\parallel = 26.7441$ a.u., $\alpha_\perp = 12.8087$ a.u.). Thus, there are only two independent fit coefficients for $\Delta V_{123}^{\text{ind}}$, one parallel and one perpendicular site polarizability. No constraints were imposed on the signs of the coefficients, which resulted in a slightly negative $\alpha_\perp$ coefficient for the site located on the C atom.

The exchange term $\Delta V_{123}^{\text{exch}}$ is represented as

$$\Delta V_{123}^{\text{exch}} = \sum_{i=1}^{5}\sum_{j=1}^{5}\sum_{k=1}^{5}\sum_{l_i l_j l_k} P_{l_i}(\cos\bar{\theta}_{1|i}) P_{l_j}(\cos\bar{\theta}_{2|j}) P_{l_k}(\cos\bar{\theta}_{3|k}) \times \left[A_{ijk}^{l_i l_j l_k} \exp\left(-aR_{123|ijk}\right) + B_{ijk}^{l_i l_j l_k} \exp\left(-bR_{123|ijk}\right) + C_{ijk}^{l_i l_j l_k} \exp\left(-cR_{123|ijk}\right)\right], \tag{13}$$

where $P_l(x)$ refers to an lth order Legendre polynomial and $R_{123|ijk} = R_{12|ij} + R_{13|ik} + R_{23|jk}$. The optimal values of the nonlinear parameters a, b, and c were found by trial and error to be 1.37 Å^{-1}, 0.85 Å^{-1}, and 0.49 Å^{-1}. For $\Delta V_{123}^{\text{exch}}$, we use five sites per molecule. Two of them are located at the ends of the molecule at a distance from the C atom of 1.33 Å (again found by trial and error), whereas the others are identical with the ones used for $\Delta V_{123}^{\text{disp}}$ and $\Delta V_{123}^{\text{ind}}$. The summation over l_i, l_j, and l_k values was restricted to all combinations that satisfy $l_i + l_j + l_k \leqslant 3$ except for $l_i = l_j = l_k = 1$ (which can be expressed using zeroth- and second-order Legendre polynomials) as well as to combinations that satisfy $l_i + l_j + l_k = 4$ with $\max(l_i, l_j, l_k) = 2$. Furthermore, the coefficients $A_{ijk}^{l_i l_j l_k}$ and $B_{ijk}^{l_i l_j l_k}$ were fixed at zero unless $l_i + l_j + l_k \leqslant 2$ and $l_i + l_j + l_k \leqslant 3$, respectively. This approach resulted in 64, 109, and 145 distinct fit coefficients $A_{ijk}^{l_i l_j l_k}$, $B_{ijk}^{l_i l_j l_k}$, and $C_{ijk}^{l_i l_j l_k}$, respectively.

The 323 independent linear parameters of the chosen analytical representation of ΔV_{123} were optimized in a least-squares fit to the 9401 *ab initio* calculated values using a weighting function w given by

$$w\left(R_{12}, R_{13}, \bar{\theta}_1, V_{12}, V_{13}, V_{23}\right) = \frac{(R_{12}^* R_{13}^*)^2 \left[\sin(\bar{\theta}_1) + 0.5\right]}{\left[1 + (V_{12}^* + 0.75)^2 + (V_{13}^* + 0.75)^2 + (V_{23}^* + 0.75)^2\right]^2}, \tag{14}$$

where $R_{ij}^* = R_{ij}/\text{Å}$ and $V_{ij}^* = V_{ij}/(1000\,\text{K})$. The denominator of this function was chosen such that the weight of configurations increases with the pair interaction energies V_{ij} decreasing towards their minimum ($V_{ij,\min} \approx -750$ K), while the numerator increases the weight of configurations that should be more likely to occur based on simple statistical (though not rigorous) arguments without considering intermolecular interactions. The pair interaction energies are those obtained as a byproduct of the calculations presented in Sec. II B.

The mean absolute error (MAE) of $\Delta V_{123}^{\text{fit}}$ is 24.6 K. However, the MAE is dominated by the most strongly repulsive configurations of three CO_2 molecules, which usually also have the highest $|\Delta V_{123}|$ values. These configurations were given a very low weight in the fit, see Eq. (14), because they are relatively unimportant for the thermodynamic properties of CO_2 in the temperature range considered in this work. For the 7996 configurations with a total interaction energy V_{123} of less than 3000 K, the MAE is only 0.32 K. In Fig. 2, the nonadditive three-body interaction energies computed using $\Delta V_{123}^{\text{fit}}$ are plotted against the corresponding *ab initio* values for these configurations. The figure shows that a large amount of cancellation between positive and negative ΔV_{123} values can be expected when calculating virial coefficients. Nevertheless, the nonadditive contribution affects the virial coefficients dramatically. For instance, it increases the third virial coefficient at room temperature by more than 60% (see Sec. III C). Therefore, the imperfection of the fit has a strong effect on the virial coefficients. For example, small changes in the functional form of the weighting function w or of the range of l_i, l_j, and l_k values for $\Delta V_{123}^{\text{exch}}$ resulted in variations of the order of 10% in the calculated values of the third virial coefficient at room temperature. The only practical solution to this problem was to vary the range of l_i, l_j, and l_k values until the resulting $\Delta V_{123}^{\text{fit}}$ yielded a VEOS that accurately reproduces pressures calculated using the empirical reference EOS of Span and Wagner[45] (hereafter denoted as SWEOS), as implemented in the CoolProp library,[46] close to room temperature at densities up to about 200 kg m^{-3}. Because of this empirical guidance, the nonadditive three-body PES presented here is not a true *ab initio* one. A Fortran 90 routine computing $\Delta V_{123}^{\text{fit}}$ is provided in the supplementary material.

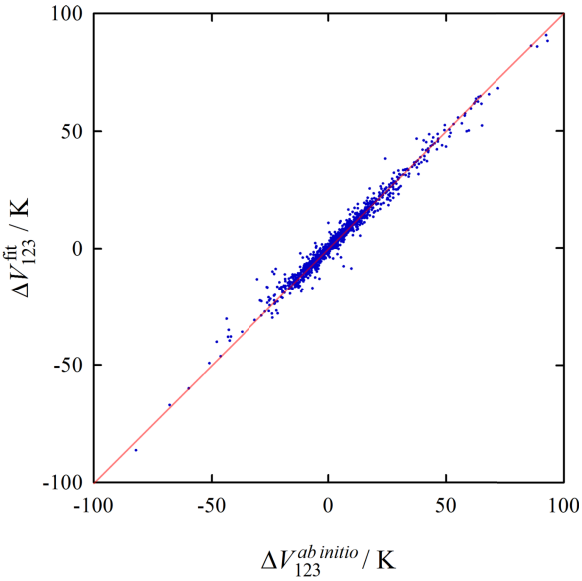

FIG. 2. Nonadditive three-body interaction energies from the fitted analytical function versus the *ab initio* calculated values for the 7996 configurations with a total interaction energy of less than 3000 K. The red line is a guide to the eye corresponding to a perfect fit.

III. VIRIAL EQUATION OF STATE

A. Calculation of the third to eighth virial coefficients

The classical third virial coefficient for a pure gas consisting of rigid molecules that interact through a pairwise-additive intermolecular potential is given as

$$B_{3,\text{add}}^{\text{cl}} = -\frac{1}{3}\int\int \langle f_{12} f_{13} f_{23} \rangle d\mathbf{R}_{12} d\mathbf{R}_{13}, \tag{15}$$

where $f_{ij} = \exp(-V_{ij}/k_B T) - 1$ is the two-particle Mayer function, k_B is Boltzmann's constant, and the angle brackets denote an average over the angular orientations of the three molecules. The nonadditive three-body contribution to the third virial coefficient, which depends on both the pair potential and the nonadditive three-body potential, was derived by Johnson and Spurling,[47]

$$\Delta B_{3,\text{nadd}}^{\text{cl}} \equiv B_{3,\text{nadd}}^{\text{cl}} - B_{3,\text{add}}^{\text{cl}} = -\frac{1}{3}\int\int\left\langle \left[\exp\left(-\frac{\Delta V_{123}}{k_B T}\right) - 1\right] e_{12} e_{13} e_{23} \right\rangle \times d\mathbf{R}_{12} d\mathbf{R}_{13}, \tag{16}$$

where $e_{ij} = f_{ij} + 1$. For the classical pairwise-additive fourth virial coefficient, the formulation of Ree and Hoover[48] was employed,

$$B_{4,\mathrm{add}}^{\mathrm{cl}} = -\frac{1}{8}\int\int\int \langle -2f_{12}f_{13}f_{14}f_{23}f_{24}f_{34} + f_{12}f_{14}f_{23}f_{34}e_{13}e_{24} + f_{13}f_{14}f_{23}f_{24}e_{12}e_{34} + f_{12}f_{13}f_{24}f_{34}e_{14}e_{23}\rangle \times d\mathbf{R}_{12}d\mathbf{R}_{13}d\mathbf{R}_{14}. \quad (17)$$

Here, the latter three terms of the integrand correspond to all distinguishable permutations of the molecule indices for one of the unlabeled cluster diagrams in the Ree–Hoover formalism of $B_{4,\mathrm{add}}^{\mathrm{cl}}$. They were used instead of $3\times f_{12}f_{14}f_{23}f_{34}e_{13}e_{24}$ for the calculations reported here to improve numerical performance. For the expression of the additive fifth virial coefficient, in terms of cluster diagrams, the reader is referred to the paper of Ree and Hoover.[48] The expressions for the nonadditive contributions to the fourth and fifth virial coefficients are given in Refs. 47 and 49, respectively.

For the calculation of the sixth to eighth virial coefficients, we used the diagrammatic formulation of Hellmann and Bich[27] because it is computationally more efficient than the Ree–Hoover formulation for these high-order virial coefficients. The Hellmann–Bich formulation can be used for both additive and nonadditive potential models. Note that there is a misprint in Eq. (63) of Ref. 27: a factor of 2 incorrectly appears in front of the fifth cluster diagram of the sixth virial coefficient; this factor should instead appear in front of the fourth diagram. The corrected equation is provided in the supplementary material.

Nuclear quantum effects were taken into account semiclassically by replacing the pair potential by the quadratic Feynman–Hibbs (QFH) effective one.[50] For two identical rigid linear molecules, the QFH potential takes the form

$$V_{12}^{\mathrm{QFH}} = V_{12} + \frac{\hbar^2}{12k_{\mathrm{B}}T}\left[\frac{1}{m}\left(\frac{\partial^2 V_{12}}{\partial x_{12}^2} + \frac{\partial^2 V_{12}}{\partial y_{12}^2} + \frac{\partial^2 V_{12}}{\partial z_{12}^2}\right) + \frac{1}{2I}\left(\frac{\partial^2 V_{12}}{\partial \psi_{1,a}^2} + \frac{\partial^2 V_{12}}{\partial \psi_{1,b}^2} + \frac{\partial^2 V_{12}}{\partial \psi_{2,a}^2} + \frac{\partial^2 V_{12}}{\partial \psi_{2,b}^2}\right)\right], \quad (18)$$

where m and I are the molecular mass and moment of inertia, respectively, x_{12}, y_{12}, and z_{12} are the Cartesian components of $\mathbf{R}_{12}$, and the angles $\psi_{1,a}$, $\psi_{1,b}$, $\psi_{2,a}$, and $\psi_{2,b}$ correspond to rotations of the molecules around their principal axes. The second derivatives in this expression were computed analytically. The QFH modification of the nonadditive three-body potential was not considered in this work.

The total nth-order virial coefficients $B_{n,\mathrm{nadd}}^{\mathrm{QFH}}$ were calculated for $n = 3$ to $n = 7$ as sums of the classical additive contributions, the classical nonadditive contributions, the QFH corrections for the additive contributions, and partial QFH corrections for the nonadditive contributions that account only for the QFH modification of the pair potential. Thus,

$$B_{n,\mathrm{nadd}}^{\mathrm{QFH}} = B_{n,\mathrm{add}}^{\mathrm{cl}} + \Delta B_{n,\mathrm{nadd}}^{\mathrm{cl}} + \Delta B_{n,\mathrm{add}}^{\mathrm{QFH}} + \Delta B_{n,\mathrm{nadd}}^{\mathrm{QFH}}, \quad (19)$$

where

$$\Delta B_{n,\mathrm{nadd}}^{\mathrm{cl}} \equiv B_{n,\mathrm{nadd}}^{\mathrm{cl}} - B_{n,\mathrm{add}}^{\mathrm{cl}}, \quad (20)$$

$$\Delta B_{n,\mathrm{add}}^{\mathrm{QFH}} \equiv B_{n,\mathrm{add}}^{\mathrm{QFH}} - B_{n,\mathrm{add}}^{\mathrm{cl}}, \quad (21)$$

$$\Delta B_{n,\mathrm{nadd}}^{\mathrm{QFH}} \equiv B_{n,\mathrm{nadd}}^{\mathrm{QFH}} - B_{n,\mathrm{add}}^{\mathrm{QFH}} - B_{n,\mathrm{nadd}}^{\mathrm{cl}} + B_{n,\mathrm{add}}^{\mathrm{cl}}. \quad (22)$$

For $n = 8$, only the classical additive contribution was calculated.

The four contributions in Eq. (19) were computed using the MSMC approach of Singh and Kofke.[31] The differences defining the terms $\Delta B_{n,\mathrm{nadd}}^{\mathrm{cl}}$, $\Delta B_{n,\mathrm{add}}^{\mathrm{QFH}}$, and $\Delta B_{n,\mathrm{nadd}}^{\mathrm{QFH}}$, Eqs. (20)–(22), were calculated directly by averaging the respective differences of the integrands at each MC step, resulting in greatly reduced statistical errors for the three correction terms. A similar approach has been previously investigated by Shaul *et al.*[51] for the calculation of the virial coefficients of helium.

As in previous work, see, for example, Ref. 21, we performed multi-temperature simulations, in which the integrand is computed for a range of temperatures at each MC step. For $B_{n,\mathrm{add}}^{\mathrm{cl}}$, the absolute value of its integrand at the lowest temperature of the chosen range was used as the sampling distribution, while for $\Delta B_{n,\mathrm{nadd}}^{\mathrm{cl}}$, $\Delta B_{n,\mathrm{add}}^{\mathrm{QFH}}$, and $\Delta B_{n,\mathrm{nadd}}^{\mathrm{QFH}}$, the absolute values of the integrands of $B_{n,\mathrm{nadd}}^{\mathrm{cl}}$, $B_{n,\mathrm{add}}^{\mathrm{QFH}}$, and $B_{n,\mathrm{nadd}}^{\mathrm{QFH}}$, respectively, at the lowest temperature were used.

In each MC step, one CO_2 molecule was displaced and rotated. The maximum step sizes for the moves were adjusted in short equilibration periods to achieve acceptance rates of 50%. To avoid unphysical negative interaction energies at very small intermolecular separations, the two-body potential was set to infinity when the C–C separation was smaller than 1.75 Å or when any of the site-site distances between the two molecules were smaller than 1 Å. The nonadditive three-body potential was set to zero when the distance between any two of its sites on different molecules was smaller than 2 Å or when any of the three C–C separations exceeded 30 Å.

In all MSMC calculations, the hard-sphere (HS) fluid with a sphere diameter of 4.5 Å was employed as reference system. The full HS virial coefficients[52] and the respective integrands were used for $n < 6$, whereas for $n \geqslant 6$, in order to save CPU time, the HS integrand consisted only of the cluster diagram (including its sign) that represents the sum of distinguishable permutations of linear chains of two-particle Mayer functions in the Hellmann–Bich formulation.[27] For $n = 6$, this is the last cluster diagram in the corrected expression given in the supplementary material. The resulting reference integrals for $n \geqslant 6$, including the overall prefactors of the corresponding virial coefficients, are equal to $(n-1)\left(2B_2^{\mathrm{HS}}\right)^{n-1}/2$.

The results of numerous independent simulation runs for each contribution and temperature range were averaged. Each simulation run in turn consisted of a large number of independent simulations, which were performed in parallel with one simulation per hardware thread. The number of simulation runs and the number of MC steps per run varied depending on the order of the virial coefficient, the temperature range, and the type of contribution. The highest total number of MC steps for each contribution were performed for the lowest temperature range of B_7 (eight temperatures from 285 K to 320 K) with 256 runs of 5×10^{10} steps for $B_{7,\mathrm{add}}^{\mathrm{cl}}$, 512 runs of 5×10^{9} steps for $\Delta B_{7,\mathrm{nadd}}^{\mathrm{cl}}$, 64 runs of 5×10^{9} steps for $\Delta B_{7,\mathrm{add}}^{\mathrm{QFH}}$, and 16 runs of 5×10^{9} steps for $\Delta B_{7,\mathrm{nadd}}^{\mathrm{QFH}}$. The deviations from the mean for each contribution and temperature were used to compute the standard uncertainties of the total virial coefficients at each temperature arising from the limited number of MC steps.

TABLE I. Lowest temperature T_{min}, highest temperature T_{max}, and number of temperatures N_{temp} in each range as well as relative standard uncertainties of $B_{3,\mathrm{nadd}}^{\mathrm{QFH}}$ to $B_{7,\mathrm{nadd}}^{\mathrm{QFH}}$ and $B_{8,\mathrm{add}}^{\mathrm{cl}}$ at the lowest and highest temperatures of each range due to the MSMC simulations, denoted as $u_{\mathrm{r,min}}$ and $u_{\mathrm{r,max}}$.

	T_{min} (K)	T_{max} (K)	N_{temp}	$u_{\mathrm{r,min}}$ (%)	$u_{\mathrm{r,max}}$ (%)
B_3	190	2000	81	0.010	0.007
B_4	230	2000	73	0.041	0.030
B_5	255	395	31	0.25	0.21
	400	2000	37	0.19	0.027
B_6	270	340	16	0.88	1.6
	345	540	24	1.7	0.22
	560	2000	24	0.18	0.049
B_7	285	320	8	15	95
	330	400	8	21	2.6
	425	700	8	3.2	1.3
	800	2000	8	0.71	0.29
B_8	600	650	2	46	25
	700	750	2	24	14
	800	2000	8	14	3.5

Table I lists the temperature ranges used for each virial coefficient, the number of temperatures in each range, and the relative standard uncertainties of $B_{3,\mathrm{nadd}}^{\mathrm{QFH}}$ to $B_{7,\mathrm{nadd}}^{\mathrm{QFH}}$ and $B_{8,\mathrm{add}}^{\mathrm{cl}}$ at the lowest and highest temperatures of each range. As expected, obtaining precise estimates of the virial coefficients becomes increasingly difficult with increasing order n and decreasing temperature. Therefore, we have not attempted to calculate the eighth virial coefficient below 600 K. Note that the strikingly high relative standard uncertainty of $B_{7,\mathrm{nadd}}^{\mathrm{QFH}}$ at 320 K is due to a sign change at about 310 K.

B. Analytical fits

The coefficients of the following analytical function were fitted to the calculated $B_{n,\mathrm{add}}^{\mathrm{cl}}$, $B_{n,\mathrm{nadd}}^{\mathrm{cl}}$, and $B_{n,\mathrm{nadd}}^{\mathrm{QFH}}$ values as well as to the B_2^{cl} and B_2^{QFH} values of Ref. 9:

$$\frac{B_n(T)}{\left(\mathrm{cm^3\,mol^{-1}}\right)^{n-1}} = b_{n,-1/2}(T^*)^{-1/2} + \sum_{k=-11}^{1} b_{n,k}(T^*)^k, \qquad (23)$$

where $T^* = T/(500\,\mathrm{K})$, and the coefficients $b_{2,-11}$ to $b_{2,-8}$, $b_{3,-11}$, $b_{3,-10}$, $b_{4,-11}$, $b_{5,-11}$, and $b_{8,-11}$ to $b_{8,-4}$ were fixed at zero. Each point was weighted with the squared inverse of its standard uncertainty. The fitted coefficients $b_{n,k}$ for the different levels of theory are provided in the supplementary material. The deviations of the fitted values of the virial coefficients from the calculated ones rarely exceed the standard uncertainties of the latter.

C. The third virial coefficient of carbon dioxide

In Fig. 3, the $B_{3,\mathrm{add}}^{\mathrm{cl}}$, $B_{3,\mathrm{nadd}}^{\mathrm{cl}}$, and $B_{3,\mathrm{nadd}}^{\mathrm{QFH}}$ values obtained in this work are compared with B_3 values calculated by Schultz *et al.*,[53] B_3 values derived from the experimentally based SWEOS,[45] and selected experimental B_3 data.[54–60] The values of Vukalovich and Masalov[54] are those quoted in Ref. 61. The figure shows that the differences between the additive and nonadditive values are dramatic, whereas the QFH correction for nuclear quantum effects is almost negligible, confirming observations from previous studies.[15,53,62]

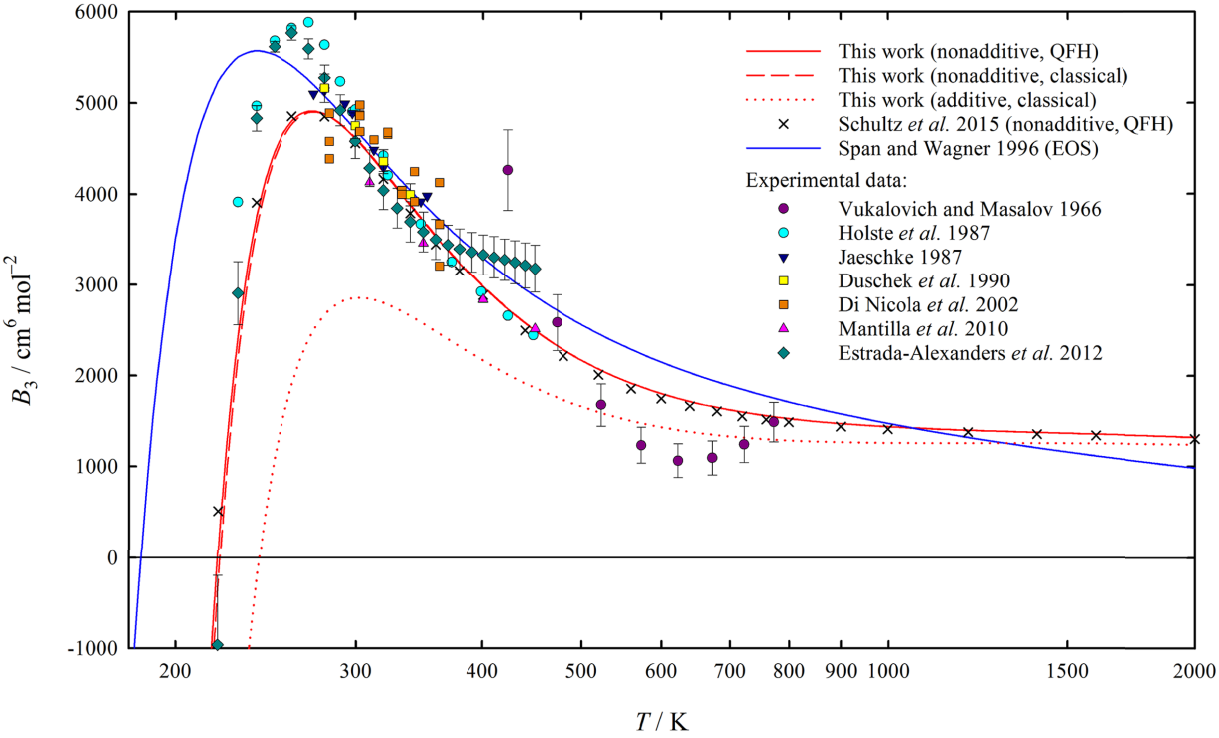

FIG. 3. Third virial coefficient B_3 as a function of temperature obtained in this work at three different levels of theory as well as B_3 values calculated by Schultz *et al.*,[53] B_3 values derived from the experimentally based SWEOS,[45] and selected experimental B_3 data.[54–60]

Schultz *et al.*[53] obtained their B_3 values using the same pair potential as in the present work[9] including the QFH correction. To account for nonadditive three-body interactions, they used an isotropic ATM term and a single polarizable site with isotropic polarizability. They did not adjust the parameters of their model to experimental B_3 data. Figure 3 shows that their values agree very well with the present $B_{3,\mathrm{nadd}}^{\mathrm{QFH}}$ values, which is somewhat surprising in view of their simple ΔV_{123} model. Even at 190 K, the lowest common temperature, the present value of $-23\,778\ \mathrm{cm^6\ mol^{-2}}$ and that of Schultz *et al.* of $-22\,406\ \mathrm{cm^6\ mol^{-2}}$ (both outside the range of the figure) are still in fairly good agreement.

The B_3 values derived from the SWEOS[45] differ substantially from the calculated values and most of the experimental data except near room temperature. This is not surprising because Span and Wagner[45] did not explicitly include experimental B_3 data in the fit of their EOS.

The experimental B_3 data of Holste *et al.*,[55] Jaeschke,[56] Duschek *et al.*,[57] Di Nicola *et al.*,[58] and Mantilla *et al.*[59] agree well with the calculated $B_{3,\mathrm{nadd}}^{\mathrm{QFH}}$ values above room temperature, whereas the maximum of B_3 at about 270 K is distinctly more pronounced in the experimental data of Holste *et al.*[55] and Estrada-Alexanders *et al.*[60] than in the values of the present work, of Schultz *et al.*,[53] of Jaeschke,[56] and of Di Nicola *et al.*[58] The temperature dependencies of the data of Estrada-Alexanders *et al.*[60] above 350 K and of the data of Vukalovich and Masalov[54,61] are clearly incorrect.

D. Higher virial coefficients of carbon dioxide

Figure 4 shows the $B_{n,\mathrm{add}}^{\mathrm{cl}}(T)$ and $B_{n,\mathrm{nadd}}^{\mathrm{QFH}}(T)$ curves obtained using Eq. (23) for $n = 4$ to $n = 7$. The $B_{n,\mathrm{nadd}}^{\mathrm{cl}}(T)$ curves are not shown because they would be almost indistinguishable from the $B_{n,\mathrm{nadd}}^{\mathrm{QFH}}(T)$ ones. It can be seen that, as in the case of the third virial coefficient, the additive and nonadditive values differ dramatically, although the disagreement becomes less severe towards higher temperatures. The latter observation justifies that for the eighth virial coefficient, which was calculated only for temperatures from 600 K to 2000 K, the nonadditive contribution was neglected. It is interesting to note that the qualitative features of the $B_{n,\mathrm{add}}^{\mathrm{cl}}(T)$ curves are somewhat similar to those of the respective $B_n(T)$ curves for the Lennard-Jones fluid.[63,64] No experimental data are depicted in the figure because the fourth and higher virial coefficients of gases cannot be determined reliably using current experimental techniques.

E. The equation of state of carbon dioxide

To assess the quality of the calculated higher-order virial coefficients, one can directly compare pressures calculated as a function of density and temperature using a VEOS with experimental data and with pressures calculated using a reliable experimentally based EOS, such as the SWEOS.[45] It would also be possible to derive other experimentally accessible quantities (e.g., the speed of sound) from a VEOS.[65] In this work, we restrict the comparison to the pressure and compare only with the SWEOS and with the more recent high-pressure EOS of Giordano *et al.*[66] The range of validity of the latter EOS ($300 \leqslant T/\mathrm{K} \leqslant 700$, $100 \leqslant p/\mathrm{MPa} \leqslant 8000$) barely overlaps with the temperatures and densities at which the VEOS

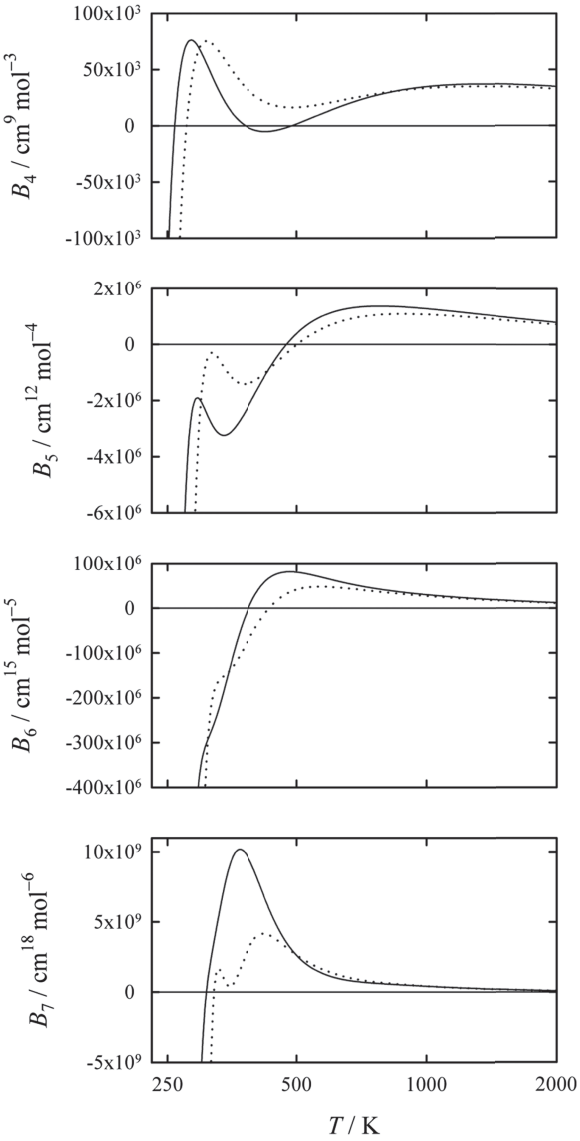

FIG. 4. Virial coefficients $B_{n,\mathrm{add}}^{\mathrm{cl}}$ (dotted lines) and $B_{n,\mathrm{nadd}}^{\mathrm{QFH}}$ (solid lines) obtained using Eq. (23) for $n = 4$ to $n = 7$ as a function of temperature.

is converged. Therefore, only limited comparison with it is possible.

Figure 5 shows the relative deviations in pressure of the analytical VEOS2 to VEOS8 at the highest level of theory as well as of the ideal gas EOS (i.e., VEOS1) from the SWEOS as a function of the mass density ρ for six temperatures. For the subcritical 275 K isotherm, the deviations are always negative and decrease in magnitude with increasing order of the VEOS up to VEOS4, whereas the inclusion of the negative fifth and sixth virial coefficients slightly worsens the agreement. The largest deviation for VEOS6 is –0.11% at the density of the saturated vapor; the uncertainty in pressure of the SWEOS at this density is about 0.02%. Contributions from the seventh and eighth virial coefficients, which were not calculated for temperatures below 285 K and 600 K, respectively, should be negligible at 275 K. For the critical isotherm, $T_c = (304.1282 \pm 0.015)$ K,[45] VEOS7 deviates by only –0.08% at a density of 200 kg m^{-3} but by –4.6% at the critical density, $\rho_c = (467.6 \pm 0.6)\ \mathrm{kg\ m^{-3}}$,[45] whereas the uncertainty in pressure of the SWEOS is always smaller than

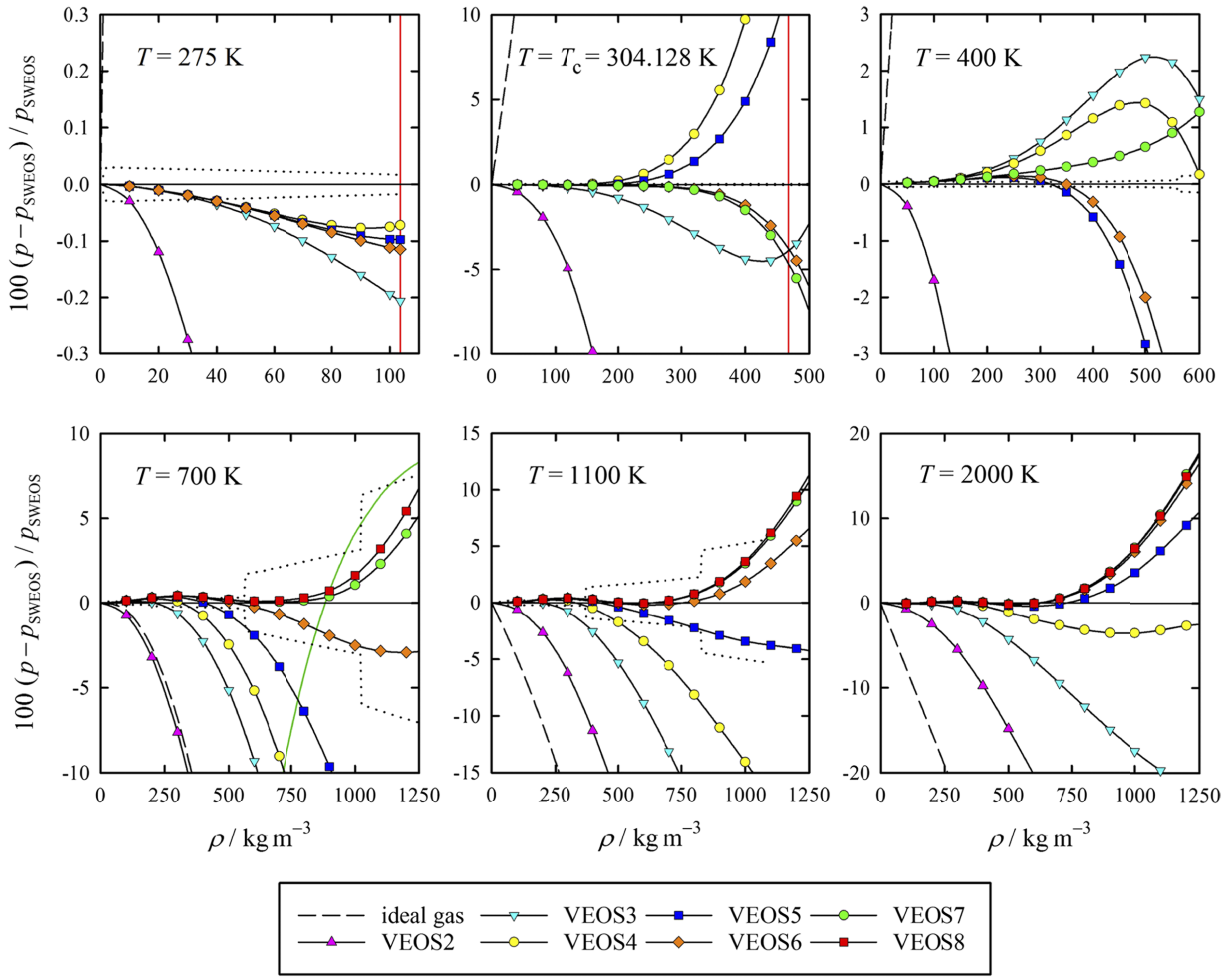

FIG. 5. Relative deviations of pressures calculated using the analytical VEOS2 to VEOS8 at the highest level of theory and the ideal gas EOS from pressures calculated using the SWEOS[45] as a function of mass density for six temperatures. Furthermore, the relative deviations of the EOS of Giordano *et al.*[66] are shown for the 700 K isotherm (solid green line). The vertical solid red lines in the upper left and upper middle panels indicate the density of the saturated vapor and the critical density, respectively, and the dotted black lines indicate the uncertainty range of the SWEOS.

0.03% for densities up to ρ_c. The very good agreement at lower densities is due to the semiempirical nature of the nonadditive three-body potential, see the last paragraph of Sec. II C. The large deviation at the critical density could be partly due to the high statistical uncertainty of the seventh virial coefficient. If $B_{7,\mathrm{nadd}}^{\mathrm{QFH}}$ is increased by its standard uncertainty, the deviations at $\rho = 200\ \mathrm{kg\,m^{-3}}$ and $\rho = \rho_c = 467.6\ \mathrm{kg\,m^{-3}}$ are only –0.07% and –2.6%, respectively. It also cannot be ruled out that the eighth and higher virial coefficients contribute significantly to the pressure at the critical density. For the supercritical isotherms, we observe that the convergence of the VEOS improves with increasing temperature. At 400 K, VEOS7 is probably converged for densities up to about 400 $\mathrm{kg\,m^{-3}}$, where it deviates by +0.38% from the SWEOS. The pressure at this density is about 21 MPa. At 700 K, 1100 K, and 2000 K, we observe deviations for VEOS8 that are within ±0.5% for densities up to 700 $\mathrm{kg\,m^{-3}}$. For higher densities, the deviations increase strongly with increasing density. At 1250 $\mathrm{kg\,m^{-3}}$, they are +6.8% at 700 K, +11.3% at 1100 K, and +17.5% at 2000 K, even though VEOS8 is well converged. The pressures calculated at this density are 834 MPa, 1309 MPa, and 2165 MPa, respectively. However, the increasing deviations go along with a similarly increasing uncertainty of the SWEOS as indicated in the figure. Note that the SWEOS is valid only for temperatures up to 1100 K and pressures up to 800 MPa. Hence, no uncertainty range is shown in the figure for the highest densities of the 1100 K isotherm and for the 2000 K isotherm.

The density ranges shown in Fig. 5 overlap with the range of validity of the EOS of Giordano *et al.*[66] only at 700 K. The figure shows that the pressures calculated using this EOS are even higher than those predicted by VEOS8 at densities above about 900 $\mathrm{kg\,m^{-3}}$, whereas increasingly negative deviations from both the SWEOS[45] and VEOS8 are observed towards lower densities.

Figure 6 shows the relative deviations in pressure of the highest-order analytical VEOS at different levels of theory from the SWEOS[45] as a function of the mass density ρ for the same six temperatures as in Fig. 5. At the lowest of the three levels, only the classical additive virial coefficients are used in the VEOS. This level of theory yields very poor agreement with the SWEOS except at the highest temperatures. At the next higher level, the nonadditive three-body contributions for the third to seventh virial coefficients are

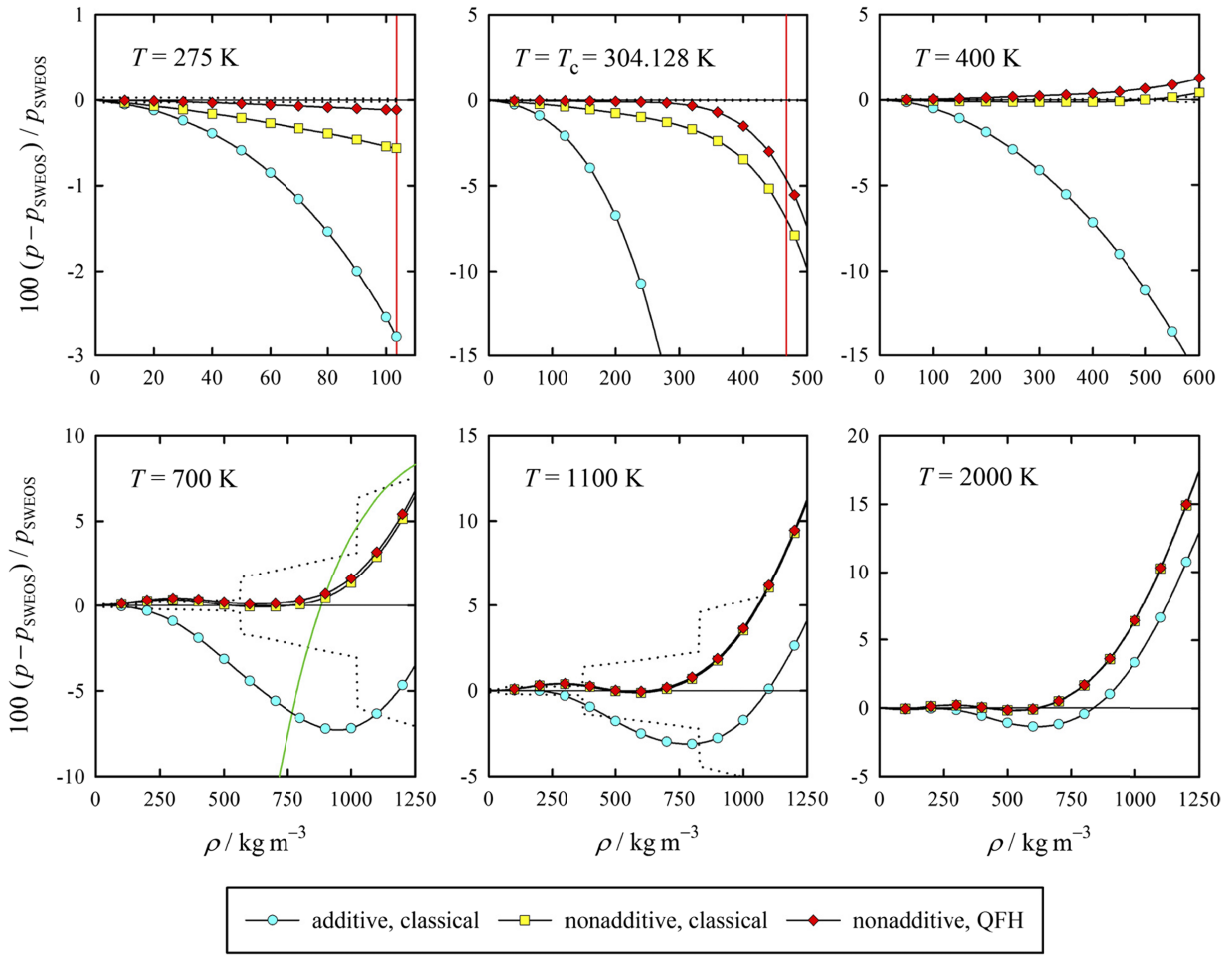

FIG. 6. Relative deviations of pressures calculated using the highest-order analytical VEOS (VEOS6 at 275 K, VEOS7 at 304.128 K and 400 K, VEOS8 at 700 K, 1100 K, and 2000 K) at different levels of theory from pressures calculated using the SWEOS[45] as a function of mass density for the same temperatures as in Fig. 5. For the meaning of the solid green, solid red, and dotted black lines, see the caption of Fig. 5.

included, which improves the agreement with the SWEOS considerably. At the highest level, which also includes the QFH correction for nuclear quantum effects for the second to seventh virial coefficients, further significant improvements can be observed for the two lowest temperatures, whereas the agreement for the 400 K isotherm deteriorates and the higher isotherms are almost unaffected by the QFH correction. It is interesting to note that at high temperatures and densities, the trends in the deviations are similar at all levels of theory, which is particularly evident for the 2000 K isotherm. Thus, the large systematic deviations at high densities are probably not related to the treatment of the nonadditive interactions or of quantum effects. If these deviations were to be caused by deficiencies in the pair potential,[9] such as its rigid nature, we would expect to see them, to some extent, already at lower densities. On the other hand, the SWEOS is based on only two experimental (p, ρ, T) data sets at the highest temperatures and densities, which is reflected in the increased uncertainty estimates given by Span and Wagner for these conditions.[45] Moreover, the comparison with the EOS of Giordano *et al.*[66] lends more support to VEOS8 than to the SWEOS. Therefore, the present VEOS8 should be accurate enough for use in the development of a new reference EOS for CO_2 to guide the behavior at high temperatures and densities. For this purpose, we provide tables of pressures calculated using VEOS8 as a function of density for 23 temperatures in the range from 900 K to 2000 K in the supplementary material. A reasonable estimate of their relative combined expanded (coverage factor $k = 2$) uncertainty U_r at all temperatures is $U_r = 0.005\% \times \rho/(\mathrm{kg\,m^{-3}})$. Pressures calculated using VEOS3 to VEOS7 are also provided to demonstrate that VEOS8 is well converged at all densities listed in the tables.

IV. SUMMARY AND CONCLUSIONS

A nine-dimensional nonadditive three-body PES for the interactions between rigid carbon dioxide molecules has been developed. It is based on counterpoise-corrected supermolecular calculations for 9401 configurations at the RI-MP2 and CCSD(T) levels of theory using basis sets up to quadruple-zeta quality. A physically motivated analytical function with terms for describing nonadditive dispersion, induction, and exchange contributions was fitted to the calculated nonadditive three-body interaction energies. Since the computed third virial coefficients turned out to be highly sensitive to the chosen functional form and to the weighting scheme applied to the PES points, the final functional form, which has 323 independent linear parameters, was selected based on a comparison

between pressures determined from calculated virial coefficients and pressures obtained from the empirical SWEOS[45] close to room temperature. For the 7996 investigated configurations with a total interaction energy of less than 3000 K, the MAE of the analytical function is 0.32 K.

The new nonadditive three-body potential was applied together with the highly accurate pair potential of Ref. 9 to calculate the virial coefficients of CO_2 up to seventh order using the MSMC approach of Singh and Kofke.[31] The calculations were performed for subcritical temperatures as well as supercritical temperatures up to 2000 K and included a semiclassical correction for nuclear quantum effects. The eighth virial coefficient was also calculated using the MSMC approach, but because of the enormous computational costs only for temperatures from 600 K to 2000 K and without taking into account nonadditive three-body contributions and quantum corrections. A simple analytical function was fitted individually to the calculated values of each virial coefficient.

The calculated values for the third virial coefficient agree very well with those of Schultz *et al.*,[53] which were calculated using the same pair potential as in the present work[9] and a very simple nonadditive three-body potential. Agreement with experimental data is, for the most part, satisfactory. However, the maximum of the third virial coefficient at about 270 K is distinctly more pronounced in two of the experimental data sets. The reasons for this discrepancy are unclear.

Pressures calculated as a function of density using VEOSs of different orders and for three different levels of theory (classical with and without nonadditive contributions and semiclassical with nonadditive contributions) were compared with the SWEOS[45] at six temperatures. For densities at which the VEOS is converged, the agreement with the SWEOS is usually within ±0.5% at the highest level of theory. Larger deviations from the SWEOS are observed near the critical point, which could be due to the high statistical uncertainty of the seventh virial coefficient and due to the neglect of higher virial coefficients. Furthermore, for temperatures above about 700 K, large positive deviations from the SWEOS occur at higher densities, which we ascribe mainly to deficiencies of the SWEOS due to the lack of accurate data for these experimentally difficult conditions.

The present results for the individual virial coefficients and for the VEOS at high temperatures could be useful for the development of a new reference EOS for carbon dioxide.

SUPPLEMENTARY MATERIAL

See supplementary material for the results of the *ab initio* calculations for the 9401 investigated configurations of three CO_2 molecules, a Fortran 90 routine computing the analytical nonadditive three-body PES, the corrected expression for the sixth virial coefficient of the formulation of Hellmann and Bich,[27] the coefficients of Eq. (23), and tables of calculated high-temperature (p, ρ, T) values.

ACKNOWLEDGMENTS

The author wishes to thank Dr. Eckard Bich (Universität Rostock) and Dr. Johann-Philipp Crusius (Imperial College London) for helpful discussions and Dr. Andrew J. Schultz (University at Buffalo) for pointing out the misprint in Eq. (63) of Ref. 27. This work was financially supported by the Deutsche Forschungsgemeinschaft (DFG), Grant No. HE 6155/1-1.

[1] K. Patkowski and K. Szalewicz, J. Chem. Phys. **133**, 094304 (2010).
[2] W. Cencek, M. Przybytek, J. Komasa, J. B. Mehl, B. Jeziorski, and K. Szalewicz, J. Chem. Phys. **136**, 224303 (2012).
[3] B. Jäger, R. Hellmann, E. Bich, and E. Vogel, J. Chem. Phys. **144**, 114304 (2016).
[4] R. Hellmann, E. Bich, and E. Vogel, J. Chem. Phys. **128**, 214303 (2008).
[5] R. Bukowski, K. Szalewicz, G. C. Groenenboom, and A. van der Avoird, J. Chem. Phys. **128**, 094314 (2008).
[6] W. Cencek, K. Szalewicz, C. Leforestier, R. van Harrevelt, and A. van der Avoird, Phys. Chem. Chem. Phys. **10**, 4716 (2008).
[7] R. J. Wheatley and A. H. Harvey, J. Chem. Phys. **134**, 134309 (2011).
[8] R. Hellmann, E. Bich, E. Vogel, and V. Vesovic, Phys. Chem. Chem. Phys. **13**, 13749 (2011).
[9] R. Hellmann, Chem. Phys. Lett. **613**, 133 (2014).
[10] R. Hellmann, E. Bich, E. Vogel, and V. Vesovic, J. Chem. Phys. **141**, 224301 (2014).
[11] F. R. W. McCourt, J. J. M. Beenakker, W. E. Köhler, and I. Kuščer, *Nonequilibrium Phenomena in Polyatomic Gases, Vol. I: Dilute Gases* (Clarendon Press, Oxford, 1990).
[12] E. Bich, J. B. Mehl, R. Hellmann, and V. Vesovic, in *Experimental Thermodynamics Volume IX: Advances in Transport Properties of Fluids*, edited by M. J. Assael, A. R. H. Goodwin, V. Vesovic, and W. A. Wakeham (The Royal Society of Chemistry, Cambridge, 2014), Chap. 7, pp. 226–252.
[13] R. Hellmann, E. Bich, and V. Vesovic, J. Chem. Phys. **144**, 134301 (2016).
[14] M. T. Oakley and R. J. Wheatley, J. Chem. Phys. **130**, 034110 (2009).
[15] K. Yu and J. R. Schmidt, J. Chem. Phys. **136**, 034503 (2012).
[16] I. Røeggen, J. Chem. Phys. **126**, 204303 (2007).
[17] W. Cencek, M. Jeziorska, O. Akin-Ojo, and K. Szalewicz, J. Phys. Chem. A **111**, 11311 (2007).
[18] W. Cencek, K. Patkowski, and K. Szalewicz, J. Chem. Phys. **131**, 064105 (2009).
[19] V. F. Lotrich and K. Szalewicz, J. Chem. Phys. **106**, 9688 (1997).
[20] A. Malijevský, F. Karlický, R. Kalus, and A. Malijevský, J. Phys. Chem. C **111**, 15565 (2007).
[21] B. Jäger, R. Hellmann, E. Bich, and E. Vogel, J. Chem. Phys. **135**, 084308 (2011).
[22] W. Cencek, G. Garberoglio, A. H. Harvey, M. O. McLinden, and K. Szalewicz, J. Phys. Chem. A **117**, 7542 (2013).
[23] E. M. Mas, R. Bukowski, and K. Szalewicz, J. Chem. Phys. **118**, 4386 (2003).
[24] Y. Wang, X. Huang, B. C. Shepler, B. J. Braams, and J. M. Bowman, J. Chem. Phys. **134**, 094509 (2011).
[25] V. Babin, G. R. Medders, and F. Paesani, J. Chem. Theory Comput. **10**, 1599 (2014).
[26] U. Góra, W. Cencek, R. Podeszwa, A. van der Avoird, and K. Szalewicz, J. Chem. Phys. **140**, 194101 (2014).
[27] R. Hellmann and E. Bich, J. Chem. Phys. **135**, 084117 (2011).
[28] K. M. Benjamin, A. J. Schultz, and D. A. Kofke, Ind. Eng. Chem. Res. **45**, 5566 (2006).
[29] K. R. S. Shaul, A. J. Schultz, D. A. Kofke, and M. R. Moldover, Chem. Phys. Lett. **531**, 11 (2012).
[30] K. Raghavachari, G. W. Trucks, J. A. Pople, and M. Head-Gordon, Chem. Phys. Lett. **157**, 479 (1989).
[31] J. K. Singh and D. A. Kofke, Phys. Rev. Lett. **92**, 220601 (2004).
[32] S. F. Boys and F. Bernardi, Mol. Phys. **19**, 553 (1970).
[33] F. Weigend and M. Häser, Theor. Chem. Acc. **97**, 331 (1997).
[34] F. Weigend, M. Häser, H. Patzelt, and R. Ahlrichs, Chem. Phys. Lett. **294**, 143 (1998).
[35] F. Weigend, M. Kattannek, and R. Ahlrichs, J. Chem. Phys. **130**, 164106 (2009).
[36] S. Kossmann and F. Neese, Chem. Phys. Lett. **481**, 240 (2009).
[37] R. A. Kendall, T. H. Dunning, Jr., and R. J. Harrison, J. Chem. Phys. **96**, 6796 (1992).
[38] F. Weigend, Phys. Chem. Chem. Phys. **4**, 4285 (2002).
[39] F. Weigend, A. Köhn, and C. Hättig, J. Chem. Phys. **116**, 3175 (2002).
[40] F. Neese, Wiley Interdiscip. Rev.: Comput. Mol. Sci. **2**, 73 (2012).

[41]CFOUR, Coupled-Cluster Techniques for Computational Chemistry, a Quantum-Chemical Program Package by J. F. Stanton, J. Gauss, M. E. Harding, P. G. Szalay with contributions from A. A. Auer, R. J. Bartlett, U. Benedikt, C. Berger, D. E. Bernholdt, Y. J. Bomble, L. Cheng, O. Christiansen, M. Heckert, O. Heun, C. Huber, T.-C. Jagau, D. Jonsson, J. Jusélius, K. Klein, W. J. Lauderdale, D. A. Matthews, T. Metzroth, L. A. Mück, D. P. O'Neill, D. R. Price, E. Prochnow, C. Puzzarini, K. Ruud, F. Schiffmann, W. Schwalbach, S. Stopkowicz, A. Tajti, J. Vázquez, F. Wang, J. D. Watts and the integral packages MOLECULE (J. Almlöf and P. R. Taylor), PROPS (P. R. Taylor), ABACUS (T. Helgaker, H. J. Aa. Jensen, P. Jørgensen, and J. Olsen), and ECP routines by A. V. Mitin and C. van Wüllen. For the current version, see http://www.cfour.de.
[42]B. M. Axilrod and E. Teller, J. Chem. Phys. **11**, 299 (1943).
[43]Y. Muto, Nippon Sugaku-Buturigakkwaishi **17**, 629 (1943).
[44]M. H. Champagne, X. Li, and K. L. C. Hunt, J. Chem. Phys. **112**, 1893 (2000).
[45]R. Span and W. Wagner, J. Phys. Chem. Ref. Data **25**, 1509 (1996).
[46]I. H. Bell, J. Wronski, S. Quoilin, and V. Lemort, Ind. Eng. Chem. Res. **53**, 2498 (2014).
[47]C. H. J. Johnson and T. H. Spurling, Aust. J. Chem. **27**, 241 (1974).
[48]F. Ree and W. Hoover, J. Chem. Phys. **41**, 1635 (1964).
[49]K. M. Benjamin, A. J. Schultz, and D. A. Kofke, J. Phys. Chem. B **113**, 7810 (2009); Erratum: **114**, 4388 (2010).
[50]R. P. Feynman and A. R. Hibbs, *Quantum Mechanics and Path Integrals* (McGraw-Hill, New York, 1965).
[51]K. R. S. Shaul, A. J. Schultz, and D. A. Kofke, J. Chem. Phys. **137**, 184101 (2012).
[52]N. Clisby and B. M. McCoy, J. Stat. Phys. **122**, 15 (2006).
[53]A. J. Schultz, D. A. Kofke, and A. H. Harvey, AIChE J. **61**, 3029 (2015).
[54]M. P. Vukalovich and Y. F. Masalov, Teploenergetika **13**, 58 (1966).
[55]J. C. Holste, K. R. Hall, P. T. Eubank, G. Esper, M. Q. Watson, W. Warowny, D. M. Bailey, J. G. Young, and M. T. Bellomy, J. Chem. Thermodyn. **19**, 1233 (1987).
[56]M. Jaeschke, Int. J. Thermophys. **8**, 81 (1987).
[57]W. Duschek, R. Kleinrahm, and W. Wagner, J. Chem. Thermodyn. **22**, 827 (1990).
[58]G. Di Nicola, G. Giuliani, F. Polonara, and R. Stryjek, Fluid Phase Equilib. **199**, 161 (2002).
[59]I. D. Mantilla, D. E. Cristancho, S. Ejaz, K. R. Hall, M. Atilhan, and G. A. Iglesias-Silva, J. Chem. Eng. Data **55**, 4611 (2010).
[60]A. F. Estrada-Alexanders, O. Guzmán, and B. Pérez-Vidal, Mol. Phys. **110**, 1349 (2012).
[61]J. H. Dymond, K. N. Marsh, R. C. Wilhoit, and K. C. Wong, in *Landolt-Börnstein: Numerical Data and Functional Relationships in Science and Technology: New Series, Group IV: Physical Chemistry*, edited by M. Frenkel and K. N. Marsh (Springer, Berlin–Heidelberg–New York, 2002) Vol. 21A, Chap. 4, p. 252.
[62]R. A. X. Persson, J. Chem. Phys. **134**, 034312 (2011).
[63]A. J. Schultz and D. A. Kofke, Mol. Phys. **107**, 2309 (2009).
[64]A. J. Schultz, N. S. Barlow, V. Chaudhary, and D. A. Kofke, Mol. Phys. **111**, 535 (2013).
[65]B. Jäger, Z. Phys. Chem. **227**, 303 (2013).
[66]V. M. Giordano, F. Datchi, and A. Dewaele, J. Chem. Phys. **125**, 054504 (2006).